



HAL
open science

New insights into the origin of fine equiaxed microstructures in additively manufactured Inconel 718

I. Cazic, Julien Zollinger, S. Mathieu, M. El Kandaoui, P. Plapper, Benoît Appolaire

► To cite this version:

I. Cazic, Julien Zollinger, S. Mathieu, M. El Kandaoui, P. Plapper, et al.. New insights into the origin of fine equiaxed microstructures in additively manufactured Inconel 718. *Scripta Materialia*, 2021, 195, pp.113740. 10.1016/j.scriptamat.2021.113740 . hal-03608596

HAL Id: hal-03608596

<https://hal.univ-lorraine.fr/hal-03608596>

Submitted on 13 Feb 2023

HAL is a multi-disciplinary open access archive for the deposit and dissemination of scientific research documents, whether they are published or not. The documents may come from teaching and research institutions in France or abroad, or from public or private research centers.

L'archive ouverte pluridisciplinaire **HAL**, est destinée au dépôt et à la diffusion de documents scientifiques de niveau recherche, publiés ou non, émanant des établissements d'enseignement et de recherche français ou étrangers, des laboratoires publics ou privés.



Distributed under a Creative Commons Attribution - NonCommercial 4.0 International License

New insights into the origin of fine equiaxed microstructures in additively manufactured Inconel 718

I. Cazic^{a,b,c}, J. Zollinger^{a,*}, S. Mathieu^a, M. El Kandaoui^b, P. Plapper^c, B. Appolaire^a

^aUniversité de Lorraine, Institut Jean Lamour, Campus ARTEM, Allée André Guinier, F-54011 Nancy, France.

^bInstitut de Soudure, 4 bd Henri Becquerel, Espace Cormontaigne, 57970 Yutz, France.

^cUniversité du Luxembourg, Campus Kirchberg, 6 rue R. Coudenhove-Kalergi, L-1359 Luxembourg.

Abstract

Fine equiaxed grain regions are frequently observed in additively manufactured Inconel 718 alloy. Based on a grain-to-grain orientation analysis using EBSD, many assemblies of neighboring grains in these regions have been found to display multiple-twins orientation relationships sharing common $\langle 110 \rangle$ directions and exhibiting 5-fold symmetry. This is an experimental proof that the grain refinement **observed in inconel 718** is due to Icosahedral Short-Range Order (ISRO) mediated nucleation mechanism. This is the first report of ISRO-mediated nucleation of fcc nickel which widens the perspectives on the microstructures control in additive manufacturing of Ni-based superalloys.

Keywords: Icosahedral Short-Range Order, Microstructure, Additive Manufacturing, Solidification, Nickel alloys

1 Inconel 718 is a heat-treatment hardenable alloy that has been used for decades in aeronautical, aerospace and
2 nuclear industries due to its excellent fatigue and corrosion resistance up to 650°C. Hence, this alloy has been used
3 early in the development of additive manufacturing (AM) of metallic alloys [1]. Although intense research has been
4 devoted to achieve the best possible properties, controlling the grain structure established during solidification re-
5 mains critical for that purpose [2]. Solidification microstructure impacts strongly both properties and processing;
6 primary dendrite arm spacing, grain size and grain texture affect the yield strength, fracture toughness and high cy-
7 cle fatigue life, while having a grain refined equiaxed microstructure increases resistance to solidification cracking [3].

8
9 **Different strategies have been proposed to control the grain structure ensuing from solidification. Contrary to**
10 **conventional casting, it is possible with AM to play with the process parameters, such as the input energy, scanning**
11 **velocity and building strategy in order to establish thermal conditions promoting equiaxed grains, i.e. low temperature**
12 **gradients and fast solidification fronts. Along this line, the most successful solution relies on preheating the substrate,**
13 **mainly in electron beam melting (EBM) technology [4, 5, 6, 7, 8, 9, 10], and predicted as potentially efficient in other**
14 **technologies such as direct energy deposition (DED) and selective laser melting (SLM) [10]. This solution is often**
15 **associated with high energy inputs contributing to establish low temperature gradients [11]. It seems more difficult to**
16 **identify general trends for the scanning speed because the relation with the velocity of the solidification front is far**

*Corresponding author.

Email address: julien.zollinger@univ-lorraine.fr

17 from direct [10, 12, 13, 14]. The same statement can be done about the building strategies, although some success has
18 been achieved for direct laser sintering [15]. Enhancing the nucleation of new grains in the supercooled liquid pool is
19 another promising route for controlling the grain structure. Hence, solutions similar to usual practices in conventional
20 casting or welding have been identified, such as addition of grain refiners in Ti64 [16], dendrite fragmentation in
21 high entropy alloys [17] and endogenous nucleants generated by the remelting of intermetallic in Al alloys with Sc
22 [18]. In some studies using DED process, it has been suggested that partially melted powder can act as heterogeneous
23 nucleation sites and promotes equiaxed grains [9, 19].

24 In both welding and additive manufacturing technologies, fine equiaxed grains (typically $\leq 10 \mu\text{m}$) have been
25 observed by several authors for low to medium linear energy densities ranging from 0.11 J/mm (selective laser melting)
26 to 117 J/mm (direct energy deposition) in AM processes such as SLM [20, 21], DED [13, 22], EBM [23] and coaxial
27 laser-wire [24] processes. When this information is provided, the equiaxed microstructure is localised at the bottom
28 of the layer in all the AM processes mentioned below and for a wide range of scanning velocities from 3 to 1000
29 mm/s. Different explanations to the equiaxed regions have been proposed so far. Bambach *et al.* have attributed the
30 formation of equiaxed grains to local recrystallisation of the solidification microstructure [24]. Mostafa *et al.* and Choi
31 *et al.* both have explained the formation of equiaxed grains by a higher concentration of impurities in remelted areas
32 that could act as heterogeneous nucleation sites for equiaxed grains [20, 21]. Other authors have pointed the effect of
33 thermal gradient G and solidification velocity V , particularly the ratio G/V evolution during solidification that could
34 change the growth morphology [23, 22]. In addition, Parimi *et al.* have underlined the possible local fluctuations in
35 G due to Marangoni effect and in nucleation sites due to powder injection [13]. They have also shown that increasing
36 the power prevents the equiaxed microstructure to appear. Finally, they have demonstrated that the building strategy
37 does not play any role in the appearance of equiaxed microstructures, whereas increasing the power lead to a fully
38 columnar microstructure.

39 In this work, the fine equiaxed microstructure observed in AM Inconel 718 was reproduced using a coaxial laser-
40 wire process. Based on detailed EBSD analysis, it is shown that the fine equiaxed grain regions consists of several
41 assembly of nearest-neighbour grains having multiple-twins orientation relationship with a common $\langle 110 \rangle$ direction
42 leading to a 5-fold symmetry and compatible with an icosahedron. This is the signature of the Icosahedral Short-
43 Range Order (ISRO) mediated nucleation mechanism revealed by Kurtuldu *et al.* in Al-based and Au-based alloys
44 [25, 26]. This makes nickel the third fcc metal where such ISRO-mediated nucleation mechanism can operate, leading
45 to a drastic reduction of the solidification grain size. It opens new prospects for obtaining fully equiaxed additively
46 manufactured parts.

47
48 Samples of $150 \times 27 \times 7 \text{ mm}^3$ of Inconel 718 alloy were manufactured using a common commercially available
49 Inconel 718 wire for welding applications (1.2 mm diameter). A Precitec CoaxPrinter laser head was used with a
50 continuous laser beam to create an annular spot focused on the substrate, where the wire is coaxially fed into the
51 melt pool, allowing to deposit the alloy layer by layer. Laser power of 2000 W, scanning speed of 1.2 m/min and

52 wire feeding rate of 2 m/min were used for laser and wire metal deposition of the samples. Each deposited layer
 53 is in average 1 ± 0.2 mm in height. The laser source is a IPG 10 kW Yb^{3+} - doped fibre solid-state laser with an
 54 operating wavelength of 1070 nm. The samples were deposited in an inert gas (Ar) atmosphere along a continuous
 55 bidirectional scanning strategy using an ABB IRB 6640-185 robot. The bidirectional scanning strategy consists in
 56 alternating building direction between each layer. Samples were cut in the x-z plane, z being the building direction
 57 and y the laser scanning direction, and prepared for both electron microscopy and electron back-scattered diffraction
 58 (EBSD) analysis by polishing respectively with 3 and 1 μm diamond solution then 0.5 μm Silica suspension (OPS).
 59 These analysis were performed with 20 kV on a Zeiss Gemini SEM500 equipped with an Oxford Instrument Symme-
 60 try camera for high resolution maps. EBSD analysis were performed with a 300 nm step for macro mapping, and 200
 61 nm step for micro mapping.

62

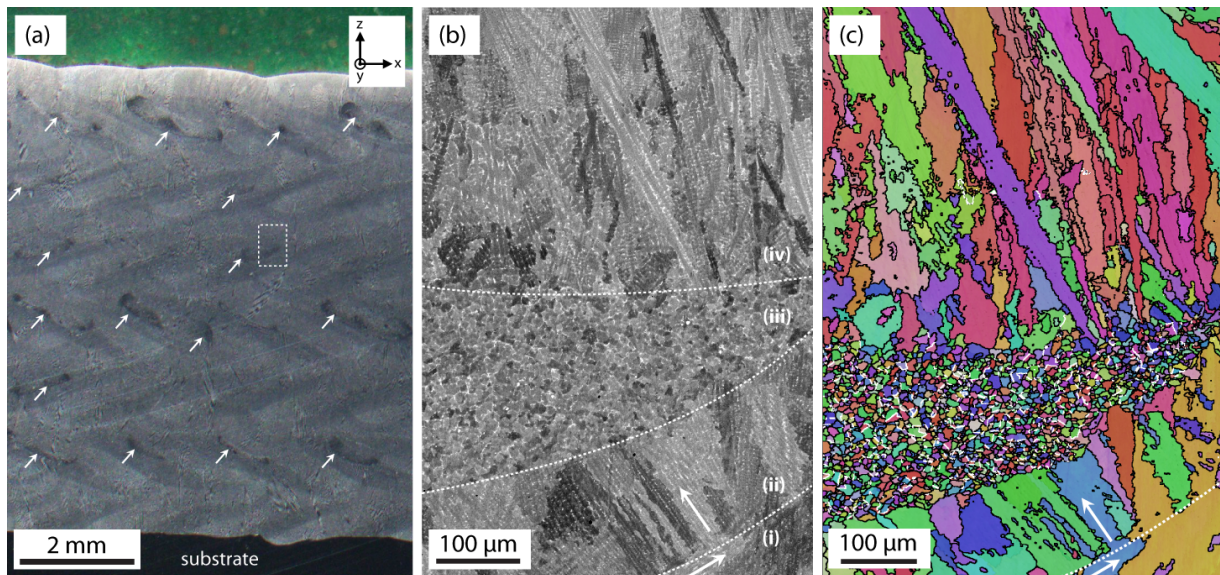


Figure 1: (a) OM in the x-z plane of the deposited beads of Inconel 718, (b) SEM-BSE image corresponding to the dashed rectangle in (a), (c) EBSD false-color map of (b). The white arrows in (a) correspond to the equiaxed zone areas. (i-iv): see text for details.

63 Figure 1(a) shows an optical micrograph (OM) in the x-z plane, y being the laser scanning direction. The macro-
 64 scopic "zigzag" grain structure is typical from bidirectional deposition [13]. Some areas, indicated by white arrows
 65 in the figure, appears in darker contrast and correspond to the fine equiaxed microstructure areas. In order to confirm
 66 that the grains are indeed equiaxed and not rotated columnar dendrites following the thermal gradient in the y-z plane
 67 of the molten pool, OM were taken in the y-z plane containing the scanning direction (not shown). The micrographs
 68 confirm that the fine grains are equiaxed, and surprisingly we have found that they form a continuous layer in the
 69 y direction. One of the equiaxed zones is shown in more details in Figure 1(b) on a SEM-BSE image. The area
 70 corresponds to the white dashed rectangle in Figure 1(a). Four distinct zones can be observed: (i) the $n - 1$ layer in

71 which growth direction is indicated by an arrow; (ii) columnar growth in the n^{th} layer by epitaxy from layer $n - 1$
72 where the change of growth direction is indicated with a white arrow; (iii) columnar-to-equiaxed transition leading
73 to a fine equiaxed microstructure; (iv) equiaxed-to-columnar transition in which oriented growth leads to a columnar
74 microstructure. Figure 1(c) is the false-colour EBSD map corresponding to Figure 1(b) where the different transitions
75 are clearly visible. In this figure, identified twin grain boundaries are outlined with white lines whereas random grain
76 boundaries (GB) with a misorientation > 10 deg. are shown with black lines: the twin boundaries are only detected
77 in the equiaxed zone. The distributions of the grain size and orientation have been obtained from the EBSD and
78 grain data. Table 1 shows the average grain size deduced from EBSD measurements and the relative twin frequency.
79 For columnar grains, the minimum Feret diameter was chosen to evaluate the grain size since their length can vary
80 significantly depending on the observation plane. The columnar grains are $\approx 37 \mu\text{m}$ in width and their length can
81 reach hundreds of micrometers, or even millimeters. The equiaxed zone shows a significant grain refinement with a
82 size $< 5 \mu\text{m}$. Moreover, the twin frequency is about 1.3% in the columnar zone, close to the value in a MacKenzie
83 distribution [27]. On the contrary, it is about 13% in the equiaxed zone, close to the value reported by Kutuldu et al.
84 when 200 ppm Ir is added to **Au-Cu-Ag** alloys in which an ISRO-mediated nucleation mechanism has been demon-
85 strated [26]. In order to prove that this nucleation mechanism is similar to that identified in Al-Zn-Cr alloys [25] and
86 Au-Cu-Ag-Ir alloys [26, 28], multiple-twin orientation relationships between several fcc grains must be identified.

87 Several aggregates of nearest-neighbour grains having multiple-twin orientation relationships (OR) have been
88 found in the equiaxed zone. Figure 2(a) shows an assembly of grains in twinning orientation relationships, obtained
89 from an high-resolution EBSD map, and labeled from 1 to 7. The $\langle 110 \rangle$ pole figures showing their mutual twin ori-
90 entations are given in Figure 2(b-d) where the red arc of a circle is the trace of their common $\{111\}$ plane. Between
91 each pair of grains in Figure 2(b), the common $\{111\}$ plane is rotated by 70.5 deg. around a common $\langle 110 \rangle$ direction,
92 which is indicated by the red circle where all the pole figures in (b) are superimposed. The pairs of grains 1-2, 2-3, 3-4,
93 4-5 show perfect twin orientation relationships (OR). The orientation relationship between grains 5 and 1 correspond
94 to what Kurtuldu et al. define as near-twin OR [25]: a twin OR and a rotation of about 7 to 8 deg around a common
95 $\langle 110 \rangle$ direction. This assembly of 5 grains is compatible with the symmetry of a decahedron with grains 1 and 5
96 that accommodate the default aperture angle of 7.5 deg. This rotation corresponds to the cumulated angle difference
97 between 5 tetrahedra of the icosahedron (360 deg) and 5 regular $\{111\}$ tetrahedra of the fcc structure (352.5 deg) [29].

Table 1: Grain sizes and twin frequencies for the columnar and equiaxed regions. For columnar grains, the grain size corresponds to the width of the grain corresponding to the minimum Feret diameter.

	Columnar region	Equiaxed region
Twin frequency (%)	1.3	12.8
Grain size (μm)	37.76 ± 7.14	4.54 ± 3.62

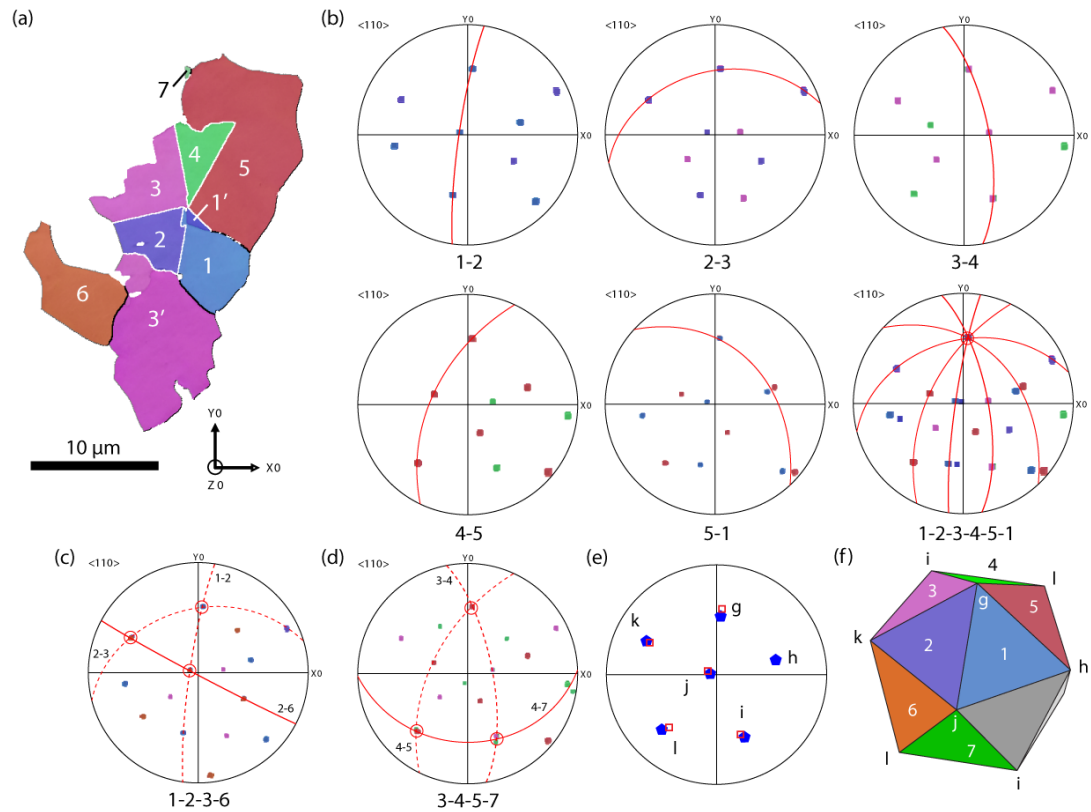


Figure 2: (a) EBSD map of seven nearest-neighbour grains with multiple-twin orientation relationships taken from the equiaxed zone. The $\langle 110 \rangle$ pole figures in (b) shows the orientation relationships between pairs of grains, and the red arcs of a circle correspond to the trace of the common $\{111\}$ plane (they are all drawn in the last pole figure). (c-d) $\langle 110 \rangle$ pole figures of grains 1-2-3-6 and 3-4-5-7. At the crossing of common $\{111\}$ twin planes, there are 3 common $\langle 110 \rangle$ directions for grains 1-2-3, 1-2-6, 2-3-6 and 3-4-5, 3-4-7, 4-5-7, respectively. (e) Stereographic projections of the 5 common $\langle 110 \rangle$ directions of the fcc grains found (red squares), together with the calculated stereographic projection of the fivefold symmetry axes of the icosahedron (blue pentagons). (f) A perfect icosahedron with facets from which the fcc phase formed have the same colour and number as the grains in (a) and 5-fold axis have the same letter as in (e).

98 2 other grains were found to feature twinning OR with one of the 5 grains presented in the figure, and 4 additional
 99 $\langle 110 \rangle$, common to at least 3 grains, were found, as shown in Figure 2(c) and (d). The grain labeled 6 displays a twin
 100 OR with grain 2 and share a common $\langle 110 \rangle$ axis with grain 1 and 3; the grain labeled 7 displays a twin OR with grain
 101 4 and share a common $\langle 110 \rangle$ axis with grain 3 and 5. Grains 6 and 7 have a near-twin OR (not represented in the
 102 figure). The $\langle 110 \rangle$ pole figure in Figure 2(e) shows the 5 common $\langle 110 \rangle$ directions of the fcc grains, together with the
 103 calculated stereographic projection of the fivefold symmetry axes of the icosahedron. A perfect icosahedron is also
 104 shown in Figure 2(f) with facets that have given rise to the fcc grains with the same color and number in Figure 2(a).
 105 This confirms as in Al-based and Au-based alloys that ISRO-mediated nucleation mechanism applies for fcc Nickel
 106 in Inconel 718 alloy.

107

108 In Al-Zn and Au-Cu-Ag alloys, the occurrence of ISRO in the liquid is induced by minute additions of Cr and Ir,
109 respectively. Approximant phases exhibiting icosahedral building blocks have been found in the Al-Cr system [30] as
110 well as a few Au-rich Tsai-type icosahedral quasicrystals (i-QC) [28], but there is no known Ni-rich i-QC. Also, no
111 specific element has been added and the microstructures have been obtained in this work with a commercial Inconel
112 718 wire. As shown by Zollinger *et al.* [28], rapid processing of ISRO-containing alloys can lead to a spinodal-like
113 decomposition of the liquid phase, leading to local heterogeneities in the liquid phase. The effect of ISRO on hetero-
114 geneous local ordering has also been evidenced by ab-initio molecular dynamics simulations in Al-Zn-Cr [31]. In the
115 present work, the local heterogeneity leading to icosahedral clusters in the liquid may not be intrinsic, i.e. induced by
116 a specific chemical element (such as Cr additions in Al-Zn alloys leading to Cr-centered icosahedra [31]), but induced
117 by the rapid melting and solidification conditions inherent to AM processes. With heating rate in the general range of
118 1 to $8 \cdot 10^4$ K/s [32], the $n - 1$ layer that partially remelt has little time for the ordered fcc phase to disordered liquid
119 transition that could lead to partially disordered liquid or even metastable short-range order configurations including
120 a certain fraction of ISRO. This hypothesis can be corroborated by an analysis based on the columnar-to-equiaxed
121 transition (CET). According to Hunts steady state model [33], the CET mainly depends on three factors: the thermal
122 gradient G , the solid/liquid interface velocity V and the number of potent nucleants ahead of the columnar front. Such
123 analysis has been performed for AM Inconel 718 by Raghavan *et al.* for electron-beam melting process [6]. Based on
124 a heat-transfer model and considering a constant nucleation density of $2 \cdot 10^{15}$ nucleus.m⁻³, the authors showed that
125 CET is more likely to occur at the end of the solidification of the layer, i.e. close to the free surface. Contrariwise,
126 the high G and low V at the interlayer boundary is not favorable to a CET. Yet this is the position where the CET
127 has been observed in this work, about 100 μ m from the interlayer boundary. Assuming the G - V path determined by
128 Raghavan *et al.* is valid, this means that the number of potent nucleus varies in the layer thickness, and is much more
129 significant close to the interlayer boundary where the liquid phase comes from remelting of the $n - 1$ layer. From the
130 twin frequency measured in this work, and following the analysis of Kurtuldu and Rappaz [34], $\approx 13\%$ of twin GBs
131 relates to fraction of icosahedral nucleants over the total number of nucleants of 10%, each icosahedral cluster giving
132 birth to potentially 20 fcc grains. The ISRO-mediated nucleation mechanism induced by the fast melting can explain
133 why a CET occurs in high G and low V regions, by increasing strongly the local number of nucleation sites close to the
134 interlayer boundary. This shows that the melting step can be employed beyond its usual role in the building process.
135 Our explanation for the occurrence of small grains in Inconel 718 suggests a new route to refine the grain structure
136 in alloys displaying ISRO mediated nucleation, in between the current strategies based on either the control of the
137 thermal conditions [4, 5, 6, 7, 9, 10, 11], or the enhancement of nucleation [9, 16, 17, 19]. Indeed, the route based on
138 ISRO mediated nucleation requires some melting that remains to be optimized. It is similar in spirit to what has been
139 observed in Al alloys containing Sc [18], but with a different mechanism. Finally, it is worth noting that the reported
140 grain sizes associated with the ISRO mediated nucleation seem in average lower than the sizes achieved by controlling
141 the thermal conditions in Inconel 718. Even if this observation must be consolidated by quantitative comparisons, it
142 suggests that ISRO mediated nucleation is worth to be further investigated for AM of Ni base superalloys.

143

144 To conclude, Inconel 718 alloy has been additively manufactured with a laser-wire co-axial process. Multiple
145 equiaxed zones were observed in the sample. Based on detailed EBSD analysis, it has been shown that the equiaxed
146 grains ensue from an ISRO-mediated nucleation mechanism, previously observed in Al-based and Au-based fcc alloys
147 only. The icosahedral symmetry deduced from EBSD analysis of the fcc phase is expected to have originated from
148 the fast remelting of the previous layer, providing metastable configurations in the liquid favorable to the nucleation
149 of the fcc phase. These results open up new prospects for additive manufacturing of nickel based alloys. Indeed,
150 controlling the ISRO nucleation mechanism in these alloys so as to obtain homogeneously fine equiaxed grains would
151 (i) avoid solidification cracking, (ii) weaken texture to get isotropic mechanical properties, and (iii) benefit from the
152 grain refinement to increase room temperature mechanical properties.

153 Acknowledgements

154 This work was funded by the INTERREG VA "Grande Region" program "FAFIL" No. 050-4-08-126, and by
155 the ANRT France under a CIFRE Ph.D. fellowship (Grant Number 2018-1630). The authors would like to thank C.
156 Bernardi, D. Knispel and M. Schmitt for the assistance with the AM process.

157 References

- 158 [1] B. Baufeld, *J. Mater. Eng. Perform.* 21 (2012) 1416–1421.
- 159 [2] N. Raghavan, S. Simunovic, R. Dehoff, A. Plotkowski, J. Turner, M. Kirka, S. Babu, *Acta Mater.* 140 (2017) 375–387.
- 160 [3] S. Kou, *Welding metallurgy*, John Wiley & Sons, New Jersey, USA, 2003.
- 161 [4] C. Körner, H. Helmer, A. Bauereiß, R. F. Singer, in: *MATEC Web of Conferences*, volume 14, EDP Sciences, p. 08001.
- 162 [5] R. R. Dehoff, M. Kirka, W. Sames, H. Bilheux, A. Tremsin, L. Lowe, S. Babu, *Mater. Sci. Technol.* 31 (2015) 931–938.
- 163 [6] N. Raghavan, R. Dehoff, S. Pannala, S. Simunovic, M. Kirka, J. Turner, N. Carlson, S. S. Babu, *Acta Mater.* 112 (2016) 303–314.
- 164 [7] H. Helmer, A. Bauereiß, R. Singer, C. Körner, *Mater. Sci. Eng. A* 668 (2016) 180–187.
- 165 [8] M. M. Kirka, D. A. Greeley, C. Hawkins, R. R. Dehoff, *Int. J. Fatigue* 105 (2017) 235–243.
- 166 [9] S. S. Babu, N. Raghavan, J. Raplee, S. J. Foster, C. Frederick, M. Haines, R. Dinwiddie, M. Kirka, A. Plotkowski, Y. Lee, et al., *Metal. Mater.*
167 *Trans. A* 49 (2018) 3764–3780.
- 168 [10] P. Liu, Z. Wang, Y. Xiao, M. F. Horstemeyer, X. Cui, L. Chen, *Addit. Manuf.* 26 (2019) 22–29.
- 169 [11] M. M. Kirka, Y. Lee, D. A. Greeley, A. Okello, M. J. Goin, M. T. Pearce, R. R. Dehoff, *Jom* 69 (2017) 523–531.
- 170 [12] G. L. Knapp, N. Raghavan, A. Plotkowski, T. Debroy, *Addit. Manuf.* 25 (2019) 511–521.
- 171 [13] L. L. Parimi, G. Ravi, D. Clark, M. M. Attallah, *Mater. Charact.* 89 (2014) 102–111.
- 172 [14] M. Zheng, C. Li, X. Zhang, Z. Ye, X. Yang, J. Gu, *Addit. Manuf.* (2020) 101660.
- 173 [15] A. Hadadzadeh, B. S. Amirkhiz, J. Li, M. Mohammadi, *Addit. Manuf.* 23 (2018) 121–131.
- 174 [16] M. Birmingham, D. StJohn, J. Krynen, S. Tedman-Jones, M. Dargusch, *Acta Mater.* 168 (2019) 261–274.
- 175 [17] S. Guan, K. Solberg, D. Wan, F. Berto, T. Welo, T. Yue, K. Chan, *Mater. Des.* 184 (2019) 108202.
- 176 [18] K. V. Yang, Y. Shi, F. Palm, X. Wu, P. Rometsch, *Scripta Mater.* 145 (2018) 113–117.
- 177 [19] B. Attard, S. Cruchley, C. Beetz, M. Megahed, Y. Chiu, M. Attallah, *Addit. Manuf.* 36 (2020) 101432.
- 178 [20] A. Mostafa, I. Picazo Rubio, V. Brailovski, M. Jahazi, M. Medraj, *Metals* 7 (2017) 196.

- 179 [21] J.-P. Choi, G.-H. Shin, S. Yang, D.-Y. Yang, J.-S. Lee, M. Brochu, J.-H. Yu, *Powder Technol.* 310 (2017) 60–66.
- 180 [22] M. Renderos, A. Torregaray, M. E. Gutierrez-Orrantia, A. Lamikiz, N. Saintier, F. Giro, *Mater. Charact.* 134 (2017) 103–113.
- 181 [23] R. C. Benn, R. P. Salva, in: *Proceedings of the 7th International Symposium on Superalloy 718 and Derivatives*, TMS, 2010, pp. 455–469.
- 182 [24] M. Bambach, I. Sizova, F. Silze, M. Schnick, *Procedia CIRP* 74 (2018) 206–209.
- 183 [25] G. Kurtuldu, P. Jarry, M. Rappaz, *Acta Mater.* 61 (2013) 7098–7108.
- 184 [26] G. Kurtuldu, A. Sicco, M. Rappaz, *Acta Mater.* 70 (2014) 240–248.
- 185 [27] J. Mackenzie, *Biometrika* 45 (1958) 229–240.
- 186 [28] J. Zollinger, B. Rouat, J. Guyon, S. Pillai, M. Rappaz, *Metall. Mater. Trans. A* 50 (2019) 2279–2288.
- 187 [29] M. Rappaz, P. Jarry, G. Kurtuldu, J. Zollinger, *Metall. Mater. Trans. A* (2020).
- 188 [30] M. Audier, M. Durand-Charre, E. Laclau, H. Klein, J. *Alloys Compd.* 220 (1995) 225–230.
- 189 [31] A. Pasturel, N. Jakse, *J. Chem. Phys.* 146 (2017) 184502.
- 190 [32] M. Ma, Z. Wang, X. Zeng, *Mater. Sci. Eng. A* 685 (2017) 265–273.
- 191 [33] J. D. Hunt, *Mater. Sci. Eng.* 65 (1984) 75–83.
- 192 [34] G. Kurtuldu, M. Rappaz, in: *IOP Conf. Ser. Mater. Sci. Eng.*, volume 84, p. 12012.

